AALBORG UNIVERSITY

Resonant-inductor-voltage feedback active damping based control for grid-connected inverters with LLCL-filters

Huang, Min; Wang, Xiongfei; Loh, Poh Chiang; Blaabjerg, Frede

Resonant-Inductor-Voltage-Feedback Active Damping Based Control for Grid-Connected Inverters With *LLCL*-filters

Min Huang, Xiongfei Wang, Poh Chiang Loh, Frede Blaabjerg

Department of Energy Technology

Aalborg University

Aalborg, Denmark

hmi@et.aau.dk, xwa@et.aau.dk, pcl@et.aau.dk, fbl@et.aau.dk

Abstract— LLCL-filter is recently emerging into grid-connected inverters due to its high attenuation of high-frequency harmonics with a smaller size. Active damping methods have been proposed to reduce the resonance peak caused by the *LLCL*-filter to stabilize the whole system without extra losses. The active damping method with an extra feedback provides a high rejection of the resonance so that the dynamic is improved. In this paper, taking a Proportional-Resonant (PR) together with a harmonic compensator (HC), resonant-inductor-voltage-feedback active damping is applied on an *LLCL*-filter based three-phase grid-connected voltage source inverter (VSI). The design method is described through the analysis in the s-domain and the z-domain. Then the robustness and harmonic rejection of the grid voltage with the active damping method is analyzed considering the processing delay. Finally, the performance of the proposed method is investigated in simulation and by experimental results.

I. INTRODUCTION

Over the last decade, the growing energy demand and greenhouse effect have prompted a renewed interest in the use of renewable energy, such as solar energy, wind energy and fuel cell, etc. Voltage Source Inverter (VSI) has increasingly been used to enable the integration of renewable power generations into grids. Due to the switching frequency harmonics produced by the Pulse-Width Modulation (PWM) of VSI, a low-pass power filter is generally inserted between the VSI and the grid to attenuate PWM harmonics to an acceptable limit. An *L*-filter or an *LCL*-filter is usually used for the low-pass filter. Compare with *L*-filter, *LCL*-filter has higher attenuation of the switching frequency harmonics and allows smaller inductance. However, to further reduce the total inductance and volume of filter an *LLCL*-filter has been reported with the 10% ~25% reduction compared to an *LCL*-filter [1], [2]. Hence, the *LLCL*-filter may become attractive for the grid-connected VSIs [3], [4].

Similarly to the *LCL*-filter, the *LLCL*-filter resonance is challenging the stability of grid-connected VSI. A direct way to dampen the filter resonance is to add a dissipative element in parallel or series with the filter inductors or filter capacitor which is called as passive damping. However this method will bring extra cost and reduces the overall system efficiency [5]-[8]. Another way is to actively dampen the resonance by introducing current or voltage feedbacks or control algorithm. Active damping methods are more flexible and lossless, but they need extra sensors and bring control complexity [9]-[12]. Moreover, the performance and the stability of control system are closely related to the ratio of the resonance frequency to the control frequency, due to the computation and PWM delays in digital control system [13] - [17]. The capacitor–current-feedback active-damping for *LCL*-filter considering the effect of the delay is studied [14]. It showed how the delay has the effect to the active damping and proposed a way to reduce the delay. At the same time, the design of active damping is also influenced by the variation of the grid impedance. The robustness of the system with *LCL*-filter based on the grid impedance variation is analyzed in [18], [19].

The stability of the *LLCL*-filter is studied in [20]. It showed when the ratio of the resonant frequency to the control frequency is high the system can be stable without damping but the system robustness is not good if the resonant frequency is around the 1/6 of the control frequency. Compare with the *LCL*-filter, the *LLCL*-filter has an extra resonant inductor which is possible also be sensed to attenuate the resonance. In this paper, resonant-inductor-voltage-feedback active damping method is analyzed for the *LLCL*-filter using integral feedback coefficient considering the effect of the delay and the grid impedance variation.

In additional to the active damping method, the Proportional-Resonant with the Harmonic-Compensation (PR+HC) controllers is also used in this paper. PR can provide larger gain at the fundamental frequency to eliminate the steady sate error compared with PI regulator and HC performs well to reject the grid harmonic distortion [21], [22].

In Section II, the model of the grid-connected inverter with the *LLCL*-filter in the s-domain is introduced. Section III shows the analysis in the z-domain. The design procedures of current control and resonant-inductor-voltage-feedback are introduced in section IV. Based on the design example in section IV, section V analyzes the robustness and grid harmonic rejection with the proposed active damping. Last, simulated and experimental results are shown to verify the proposed design method.

II. MODELING THE GRID-CONNECTED INVERTER WITH THE *LLCL*-FILTER IN THE S-DOMAIN

A. The Mathematical Model

Fig. 1 shows the topology of three-phase grid-connected inverter with *LLCL*-filter, where the parasitic resistances are ignored. The *LLCL*-filter parameters are designed according to [2]. L_1 is the inverter-side inductor, C_f is the filter capacitor, L_f is the resonant inductor, L_2 is the grid-side inductor, L_g is the grid impedance, i_1 is the inverter-side current, i_c is the capacitor current, i_g is the grid-side current, u_i is the output voltage of inverter, u_{Cf} is the output voltage of the capacitor, u_{Lf} is the output voltage of the resonant inductor, u_c is the voltage of L_f-C_f circuit and u_g is the grid voltage.

Fig. 1. Structure of the three-phase inverter with *LLCL*-filter.

The inverter system can be represented as follows (1):

$$\begin{cases} L_1 \dfrac{di_1}{dt} = u_i - u_{Cf} - u_{Lf} \\ \left(L_2 + L_g\right)\dfrac{di_g}{dt} = u_{Cf} + u_{Lf} - u_g \\ C_f \dfrac{du_{Cf}}{dt} = i_1 - i_g \\ u_{Lf} = L_f\left(\dfrac{di_1}{dt} - \dfrac{di_g}{dt}\right) \end{cases} \quad (1)$$

$$\omega_r = \frac{1}{\sqrt{\left(\dfrac{L_1\left(L_2+L_g\right)}{L_1+L_2+L_g}+L_f\right)C_f}} \quad (2)$$

The resonance frequency of the *LLCL*-filter ω_r is derived in (2). The open loop transfer functions from i_g to u_i and i_c to u_i are expressed in (3) and (4), respectively.

$$G_{u_i \to i_g}(s) = \frac{L_f C_f s^2 + 1}{C_f[L_1\left(L_2+L_g\right)+\left(L_1+L_2+L_g\right)L_f]s\left(s^2+\omega_r^2\right)} \quad (3)$$

$$G_{u_i \to i_c}(s) = \frac{\left(L_2+L_g\right)s^2}{[L_1\left(L_2+L_g\right)+\left(L_1+L_g+L_2\right)L_f]s\left(s^2+\omega_r^2\right)} \quad (4)$$

B. Model of Resonant-Inductor-Voltage-Feedback Active Damping

According to [12] different variables feedbacks are feasible for damping the resonant problem. The structure of the active damping method based on the capacitor current feedback for grid-connected inverter with the *LLCL*-filter is shown in Fig. 2 which is equal to a resistance paralleled with the capacitor for grid-connected inverter with the *LCL*-filter. K_{ic} is the capacitor current feedback coefficient. $G_d(s)$ is the delay part in series with the forward path. $G_c(s)$ is the current controller. K_{PWM} is the transfer function of the inverter bridge and i_g^* is the reference current.

Fig. 2. Block diagram of grid-side current control with capacitor current feedback

There is a correlation between the capacitor current and the resonant inductor voltage. So, an integrator feedback coefficient is required. Fig. 3 shows the control block of resonant-inductor (L_f) feedback for grid-connected inverter with *LLCL*-filter after the transformation. K_{uLf} is the resonant-inductor-feedback coefficient.

Fig. 3. Block diagram of grid-side current control with resonant-inductor-voltage feedback.

According to Fig. 3, an equivalent block diagram is obtained as shown in Fig. 4. $K_g(s)$ is the grid voltage forward coefficient after moving the branch of i_g to u_c in Fig. 3.

Fig. 4. Equivalent block diagram of grid-side current control with resonant-inductor-voltage feedback.

C. Equivalent Transformation

Fig. 4 can be transformed into the model depicted in Fig. 5 [23], [24]. $H(s)$ is the injected grid current sensor. In order

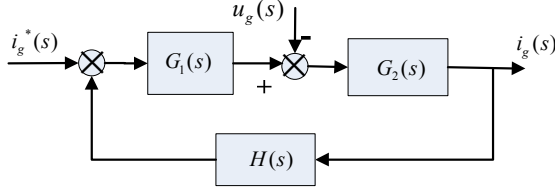to simplify the analysis, it is assumed to be one. $G_1(s)$ and $G_2(s)$ can be expressed in (5) and (6).

Fig. 5. Simplified block diagram of Fig.4.

$$G_1(s) = \frac{K_{PWM}(1+C_f L_f s^2)G_c(s)G_d(s)}{(L_1+L_f)C_f s^2 + K_{PWM}K_{uL_f}G_d(s)L_f C_f s + 1} \quad (5)$$

$$G_2(s) = \frac{(L_f+L_1)C_f s^2 + K_{PWM}K_{uL_f}G_d(s)L_f C_f s + 1}{\left[L_1(L_2+L_g)+(L_1+L_2+L_g)L_f\right]C_f s^3 + K_{PWM}K_{uL_f}G_d(s)L_f(L_2+L_g)C_f s^2 + (L_1+L_2+L_g)s} \quad (6)$$

The closed loop expression of the grid current i_g can be derived as:

$$i_g(s) = \frac{G_1(s)G_2(s)}{1+G_1(s)G_2(s)H(s)}i_g^*(s) - \frac{G_2(s)}{1+G_1(s)G_2(s)H(s)}u_g(s) \quad (7)$$

The loop gain of the system is:

$$T(s)=G_1(s)G_2(s)H(s)$$

$$= \frac{K_{PWM}(1+C_f L_f s^2)G_c(s)G_d(s)}{\left[L_1(L_2+L_g)+(L_1+L_2+L_g)L_f\right]C_f s^3 + K_{PWM}K_{uL_f}G_d(s)L_f(L_2+L_g)C_f s^2 + (L_1+L_2+L_g)s} \quad (8)$$

The system parameters are given in Table I when the inverter side current ripple is 30%, the reactive power is less than 5% of rated load, and the uppermost harmonics around the double of the switching frequency is less than 0.3% of the rated fundamental current.

TABLE I
PARAMETERS OF SYSTEM

DC link voltage U_{dc}	650 V	Grid frequency f_o	50 Hz
Grid phase voltage U_g	220 V	Resonant frequency f_r	2.6 kHz
Inductor L_1	1.8 mH	Grid-side inductor L_2	2 mH
Capacitor C_f	4 uF	Resonant inductor L_f	64 uH
Switching frequency f_s	10 kHz	Sampling period T_s	100 us

III. ANALYSIS IN THE DISCRETE DOMAIN

A. The Influence of delay for Resonant-Inductor-Voltage-Feedback Active Damping

When the grid-side current is used for feedback, the system is unstable without considering delay regardless of the controller. Because of the delay caused by the computation and PWM pattern generator, the system is no longer a minimum phase system. The stability of the system should be analyzed considering the delay. Ref. [15] - [16] have discussed the effect of the delay and methods to utilize

the delay. In this paper, to calculate these lag phase shifts the computational delay is modeled as a pure delay of T_s and the PWM is equivalent to a Zero Order Hold (ZOH), as a pure delay of $0.5T_s$.

Fig. 6 shows the bode plot of the forward path transfer function $T(s)$ with the resonant-inductor-voltage-feedback active damping based on the example in Table I. f_r is the resonant frequency and f_k is the critical frequency when the phase crosses -180º [15]. As seen in Fig. 6, the feedback of the resonant-inductor-voltage can effectively dampen the resonance peak and a larger resonant-inductor-voltage feedback coefficient leads to a better damping of the resonance peak. Delay has significant impact on the phase of the loop gain and the phase decreases at the frequencies lower than the resonance frequency. And if f_r is larger than f_k the phase of $T(s)$ will cross -180 º twice, so the resonant-inductor-voltage-feedback coefficient should be small to satisfy the magnitude margin both at the resonant frequency and the critical frequency.
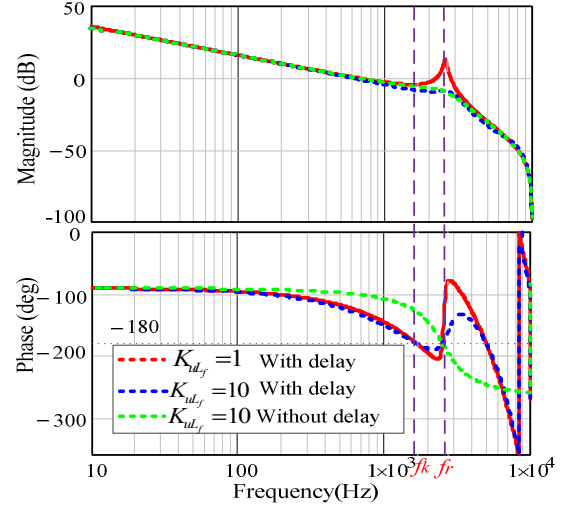

Fig. 6. Bode plot of the forward path transfer function for the single loop.

B. Analysis in the Discrete-Time Domain

For digital algorithm implementation, the proposed controller needs to be transformed from s-domain to z-domain [25]. The active damping is implemented in the digital controller, see Fig. 7.
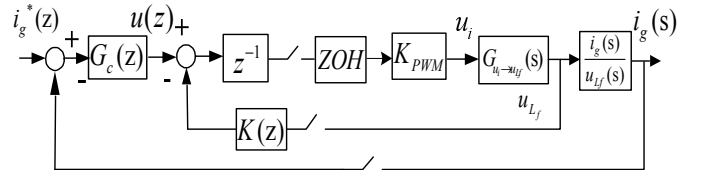

Fig. 7. Block diagram for active damping in the digital controller.

When the grid current and the resonant inductor voltage are in practice sampled at the same time instants sampling period, (3) and (4) can be transformed to z-domain by applying ZOH transform [17] to be:

$$Z_{ZOH}\left[G_{u_i \to i_g}(s)\right] = \frac{T_s}{(L_1+L_2+L_g)(z-1)} - \frac{\sin\omega_r T_s}{\omega_r(L_1+L_2+L_g)}\frac{(z-1)}{z^2-2z\cos\omega_r T_s+1}$$

$$+ \frac{\sin\omega_r T_s}{\omega_r(L_1+L_2+L_g)}\frac{(z-1)C_f L_f}{z^2-2z\cos\omega_r T_s+1} \quad (9)$$

$$Z_{ZOH}\left[G_{u_i \to i_c}(s)e^{-sT_s}\right] = \frac{(L_2+L_g)(z-1)}{[L_1(L_2+L_g)+(L_1+L_g+L_2)L_f]\omega_r}\frac{\sin\omega_r T_s}{z^2-2z\cos\omega_r T_s+1} \quad (10)$$

$$T(z) = \frac{G_c(z)z^{-1}K_{PWM}Z_{ZOH}\left[G_{u_i \to i_g}(s)\right]}{1+K_{PWM}(K_{uL_f}L_f)Z_{ZOH}\left[G_{u_i \to i_c}(s)e^{-sT_s}\right]} \quad (11)$$

where T_s is the sampling period. For *LLCL*-filter, when the switching frequency is 10 kHz, $L_f C_f$ is very small comparing to 1. The third part of (9) with can be neglected.

In the s-domain, the current controller based on PR and harmonic compensator is expressed as

$$G_c(s) = K_p + \sum_{h=1,5,7}\frac{K_{ih}s}{s^2+(\omega_0 h)^2} \quad (12),$$

where $\omega_o = 2\pi f_o$ is the fundamental angular frequency, K_p is the proportional gain, and K_{ih} is the integral gain of the individual resonant frequency h. The 5th and 7th harmonic compensations are used and they can create large impedance for grid harmonics at those frequencies. For simplicity, a discrete PR controller only at fundamental frequency ω_o is listed with forward or backward discretization [26]:

$$G_c(z) = K_p + K_{i1}\frac{-T_s z^{-2}+T_s z^{-1}}{z^{-2}+(T_s^2\omega^2-2)z^{-1}+1} \quad (13)$$

$G_c(z)$ can be reduced to K_p since the resonance gain has negligible effect above ω_o. In order to ensure that the inverter operates as a minimum-phase system over the designed operating range, their closed loop transfer functions, $1+T(z)=0$, should be explored based on (11), as shown in (14) :

$$z+K_{PWM}(K_{uL_f}L_f)Z_{ZOH}\left[G_{u_i \to i_c}(s)\right]+K_p K_{PWM}Z_{ZOH}\left[G_{u_i \to i_g}(s)\right]=0 \quad (14)$$

$T(z)$ should have no zeros and poles outside the unit circle. The root loci of the dual loop systems with active damping can be determined by plotting the denominator poles of their closed loop transfer functions as the controller gains are varied.

$$Den[z] = z^2-2z\cos\omega_r T_s+\frac{K_{PWM}K_{uLf}L_f(L_2+L_g)\sin\omega_r T_s}{\omega_r(L_1+L_2+L_g)}(z-1)+z \quad (15)$$

Based on the Routh stability criterion [17], the system is stable if no open-loop unstable poles exist.

$$\frac{(\cos\omega_r T_s-1)(L_1+L_2+L_g)}{K_{PWM}L_f(L_2+L_g)\sin\omega_r T_s} \le K_{uLf} \le \frac{(2\cos\omega_r T_s-1)(L_1+L_2+L_g)}{K_{PWM}L_f(L_2+L_g)\sin\omega_r T_s} \quad (16)$$

It can be seen from (16) when considering the delay of $1.5T_s$ the critical frequency is 1/6 of the sampling frequency. $T(z)$ has right-half plane poles if $f_r > f_s/6$. Hence, to ensure the closed-loop system stably, the resonance peak of the *LLCL*-filter should be damped below 0dB when $f_r < f_s/6$, or the resonance peak of the *LLCL*-filter should remain above 0dB when $f_r > f_s/6$ [14]. Next section will introduce the design of specific example.

IV. DESIGN OF THE CURRENT CONTROL AND RESONANT-INDUCTOR-VOLTAGE-FEEDBACK WITH *LLCL*-FILTER

A. PR+HC Controller Gain Design

The crossover frequency f_c is usually set lower 1/10 of the switching frequency considering the effect of high-frequency attenuating noise [17]. Thus the influence of the filter capacitor can be ignored when calculating the magnitude of the loop gain at f_c and the frequencies lower than f_c. The *LLCL*-filter is approximate to an *L* filter and $G_c(s)$ can be regarded as K_p at crossover frequency. K_p is determined by considering the bandwidth of the whole system and the compensated frequencies are shown in (17) and (18). The cross-over frequency ω_c can be determined in (19) considering the phase lag caused by the delay.

$$G_c(\omega_c) \approx K_p, \quad T(\omega_c) \approx \left|\frac{K_p K_{PWM}}{\omega_c(L_1+L_2)}\right| \quad (17)$$

$$\omega_c = \frac{\pi/2-\Phi_m}{3T_s/2} \quad (18)$$

$$K_p \approx \frac{\omega_c(L_1+L_2)}{K_{PWM}}, \quad (19)$$

where Φ_m is the desired phase margin. Usually, if the value of K_{ih} is larger, the steady-state error is smaller and robustness of grid frequency is better [20], but large K_{ih} would lead to poor phase margin and affects overall system performance. Hence K_{ih} should be designed to satisfy the phase margin.

B. Resonant-Inductor-Voltage-Feedback CoefficientDesign

Due to the influence of the delay, the design of resonant-inductor-voltage-feedback active damping coefficient should be complicated by the value of resonant frequency. According to Fig. 6 and (16), it can be deduced that the gain margin at f_r and $f_s/6$ is very important to the system stability when $1.5T_s$ is considered. GM_1 and GM_2 are the magnitude of $T(z)$ at f_r and $f_s/6$ that can be calculated based on (8) [17]. $GM_1 > 0$ means the magnitude is lower than 0 dB at the corresponding frequency. Then the relation between K_{uLf} and GM_1, GM_2 can be obtained as (20) and (21).

$$K_{u_{Lf}} = 10^{GM_1/20}\frac{2\pi f_c L_1}{L_f K_{PWM}} \quad (20)$$

$$K_{u_{Lf}} = 10^{GM_2/20}(\frac{6f_r}{f_s})^2\frac{2\pi f_c L_1}{L_f K_{PWM}}+\frac{2\pi f_c L_1}{L_f K_{PWM}}\frac{(f_s/6)^2-(f_r)^2}{f_s/6} \quad (21)$$

When $f_r < f_s/6$, the resonant frequency will increase with K_{uLf} increasing, then K_{uLf} should satisfy (16) to make sure the

1197

phase only across -180° once at f_r, $GM_1 > 0$. If K_{uLf} does not satisfy (16), there are unstable poles, $GM_1 > 0$ and $GM_2 < 0$; When $f_r > f_s/6$, $GM_1 < 0$ and $GM_2 > 0$ to make sure the magnitude of the loop gain at $f_s/6$ must be lower than 0 dB and at f_r must be larger than 0 dB.

C. Design Example

Taking the system given in Table I as an example, the basic design procedures can be addressed as:

1. Determine the parameters of the loop gain. According to Table I, the resonant frequency is larger than $f_s/6$, $GM_1 < 0$ and $GM_2 > 0$. The desired phase margin Φ_m should be larger than 30° and $GM_1 = $ -4dB, $GM_2 = $ 2.5dB to get a good dynamic response and stability margin.

2. Obtain the value of K_p and f_c to satisfy all the requirements according to (17), (18) and (19), $f_c=$ 1.0 kHz is chosen to obtain fast dynamic response. Then K_p is calculated as 0.06 according to (18).

3. Taking $K_p=0.06$ into the open loop $T(z)$, root locus of the system with K_{uLf} increasing can be drawn in Fig. 8 to find the satisfactory feedback gain in this example. There is a region for K_{uLf} to keep the system stable. Take $f_c = 1.0$ kHz in (20), (21) to make sure the gain margin. $K_{uLf}=110.5$ is chosen.

4. Then decide $K_{i1}= K_{i5}= K_{i7}=25$ by bode plot to get a small steady error with appropriate grid harmonic rejection.
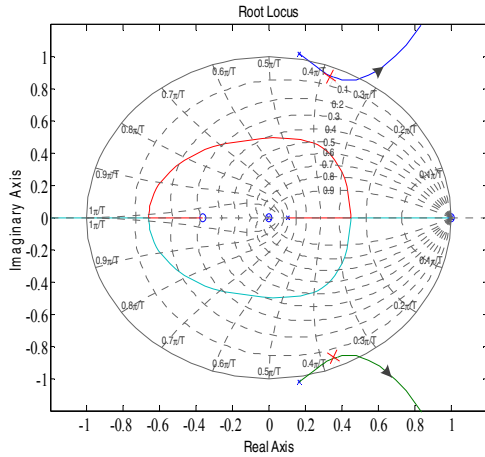
Fig. 8. Root locus of the system with K_{uLf} increasing.

V. STABILITY AND ROBUSTNESS ANALYSISES

A. Robustness Analysis With Impedance Variation

The Robustness of the system is in respect to the variation of damping coefficient, system parameters and grid transformer impedance. The system is capable of rejecting low frequency harmonic distortion, which is existing in the grid voltage. Based on the control parameters

designed before, Fig. 9 shows bode plots of system open-loop transfer function $T(s)$ under different grid inductances: 0.5 mH, 1.8 mH, and 4 mH. The gain will be decreased and the effect of the active damping will be decreased with L_g increasing, but it is still stable.
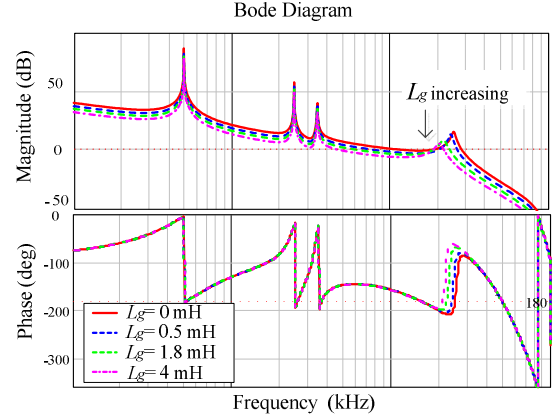

Fig. 9. System open-loop bode plots with L_g increasing.

While designing a controller, a typical specification evaluating the robustness of a system is the gain margin in root locus. The performance of the resonant-inductor-voltage-feedback active-damping control with the grid impedance variation is studied by closed-loop pole maps, as shown in Fig.10. The pair closed-loop poles introduced by the PR regulator are not drawn. With the increasing of L_g, the damping ratio of the system is reduced. The resonant poles are inside the unit circle but getting close to the border. The system has enough robustness towards the grid impedance variation in this case.
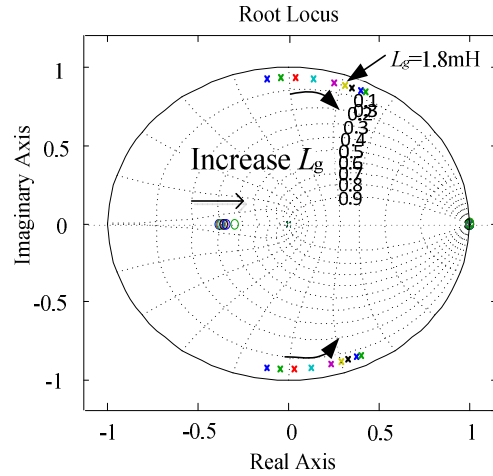

Fig. 10. Root locus of the system with L_g variation.

B. Robustness Analysis With Variation of Inductor L_f

For the LLCL-filter, L_f is designed according to the switching frequency. It can be seen from (20) and (21), the K_{uLf} is related to L_f.

When K_{uLf} is designed, if the parameter drift of L_f is in a range of ± 20%, then the actual feedback value of K_{uLf}

would also has a variation of $\pm$ 20%. This will influence the damping effect of the resonant-inductor-voltage-feedback and could cause instability. Hence when K_{uLf} is designed according to (20), (21) and the root locus of the system, the enough margins should be reserved considering the possible variation of the inductor L_f.

C. Grid Harmonics Rejection

The grid voltage is seen as the disturbance term in the design of the current loop controller. PR with HC can be utilized. The transfer function from u_g to i_g is expressed as:

$$\frac{i_g(s)}{u_g(s)} = \frac{G_2(s)}{1+G_1(s)G_2(s)H(s)} \tag{22}$$

As shown in Fig. 11, with the increase of the grid inductors, the characteristics do not change too much with the active damping. It shows the system has sufficient grid harmonic rejection capability at the compensated frequencies, 250 Hz, and 350 Hz. At the resonant frequency, the system has sufficient damping.
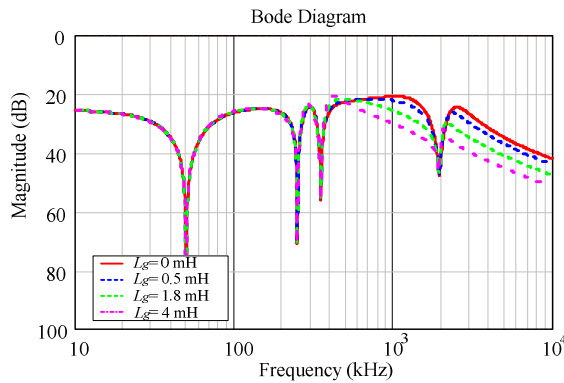
Fig. 11. Characteristic plots of grid harmonic rejection.

VI. SIMULATION RESULTS

In order to test the current control and the active damping method of *LLCL*-filter based grid-connected inverter for the stability and robustness analysis, a three-phase inverter with 6 kW rated power is simulated using MATLAB. For the integral feedback control, the noise and switching harmonics presented in the inductor current may be amplified, and therefore, a low-pass filter is normally used in practical applications, as shown in Fig.12.
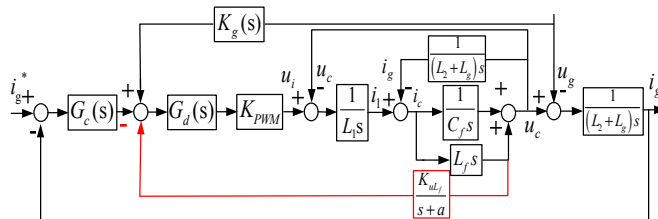

Fig. 12. Block diagram of grid-side current control with resonant inductor voltage feedback.

This paper uses PR+HC controller with resonant-inductor-voltage-feedback under the system shown in Table

I. According to the designed parameters before, some simulations can be done. The resonant frequency is 2.6 kHz which is higher than $f_s/6$. Theoretically, the system can be stable without active damping. Fig. 13 shows the dynamic performance of the grid current without active damping when change the reference peak current from 7 A to 12.9 A.
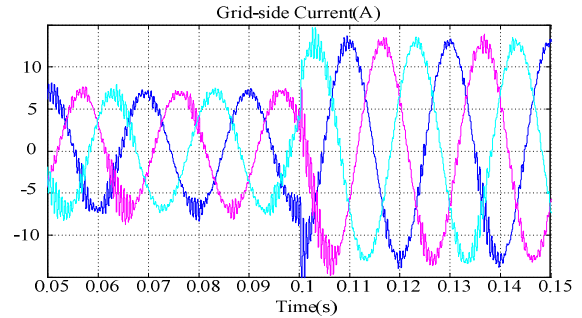

Fig. 13. Grid-side waveform without damping when change the reference current from 7A to 12.9A.

Fig. 14 shows the dynamic performance of the grid current resonant-inductor-voltage feedback when change the reference peak current from 7 A to 12.9 A. K_p=0.06 and K_{uLf}=110.5.
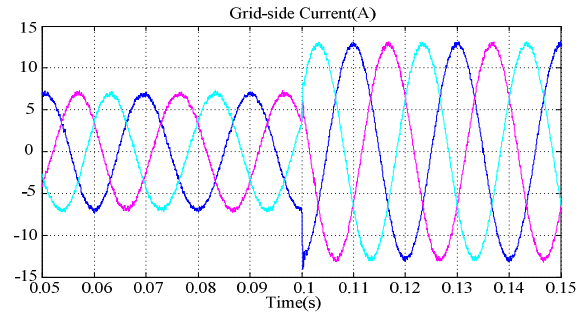

Fig. 14. Grid-side currents waveforms with active damping when change the reference current from 7A to 12.9A.

Fig. 15 shows grid-side currents waveforms when grid impedance is 4 mH. The system is unstable at the beginning without damping and become stable when resonant-inductor-voltage-feedback active damping method is enabled at the time 0.1s.
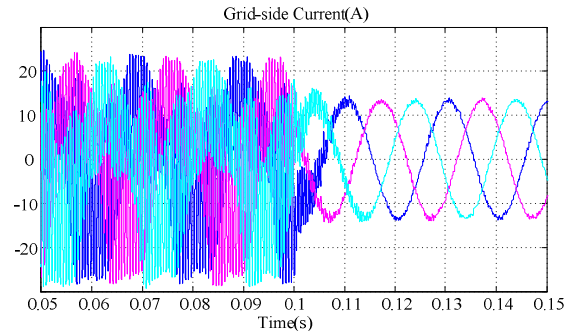

Fig. 15. Grid current waveform when active damping is enabled at time 0.1s under grid impedance is 4mH.

1199

VII. EXPERIMENTAL RESULTS

As shown in Fig. 16, the experimental setup consists of a Danfoss FC302 converter connected to the grid through an isolating transformer and the DC-link supplied by Delta Elektronika power sources. The control algorithm has been implemented in a dSPACE DS1103 real time system. The parameters of the system are shown in the Table I. The leakage inductance of the transformer is 2mH.
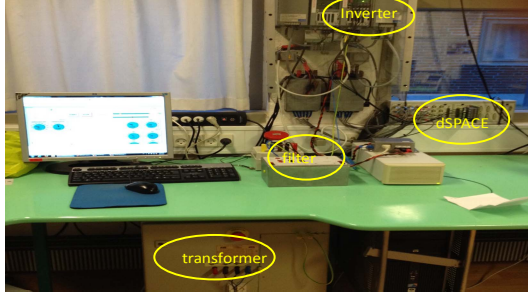

Fig. 16. Photograph of set-up for experiments with the three- phase grid-connected converter.

Fig. 17 shows the experimental results of u_c and i_g under the steady state situation with the resonant-inductor-voltage-feedback active damping.
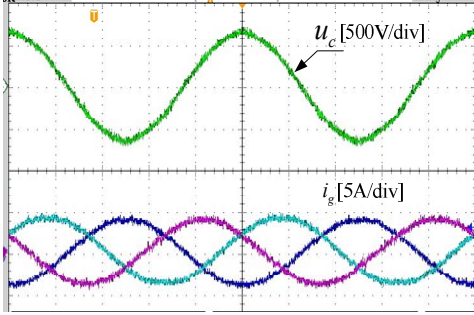

Fig. 17. Experimental results with active damping under the steady state.

Fig. 18 shows the dynamic transition of grid-side currents when the power is increased with resonant-inductor-voltage-feedback active damping.
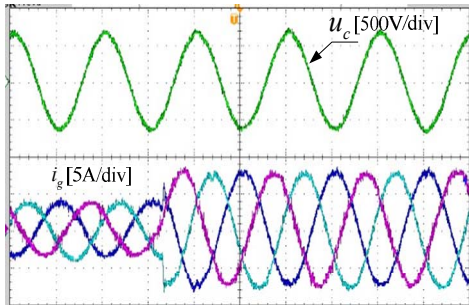

Fig. 18. Experimental results when the reference of the grid-current is increased with active damping.

Fig. 19 shows the experimental results when the active damping feedback coefficient K_{uLf} is increased and makes the system unstable. Fig. 20 shows the grid-side currents and $L_f C_f$ circuit voltage when active damping is enabled with the grid impedance is 4 mH. The system is unstable without the active damping under the influence of the grid-impedance and then become stable when the resonant-inductor-voltage-feedback is enabled.
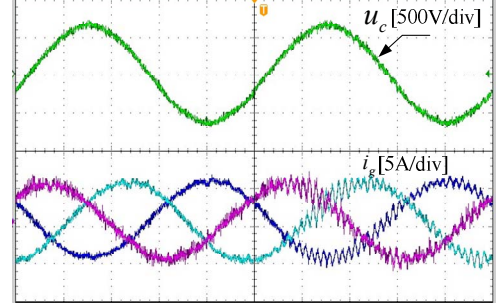

Fig. 19. Experimental results when active damping feedback coefficient K_{uLf} is increased.
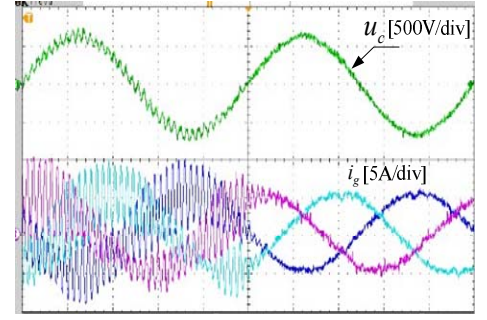

Fig. 20. Experimental results when active damping is enabled with L_g= 4 mH.

VIII. CONCLUSION

This paper has presented a resonant-inductor-voltage-feedback active damping method for *LLCL*-filter based grid-connected inverter considering the delay effect. The ratio of the resonance frequency to the control frequency has important influence on the system stability.

In order to enhance the output harmonic current rejection and reduce steady state error, PR+HC control algorithm was used in the current control. The work also shows the impact of resonant frequency on the choosing of active damping coefficient to make the system stable. The design method is given based on the analysis in the s-domain and z-domain. The analysis and the design example demonstrate a system with the resonant-inductor-voltage-feedback active damping that has a good robustness against grid impedance variation.

REFERENCES

[1] W. Wu, Y. He, and F. Blaabjerg, "An LLCL power filter for single-phase grid-tied inverter," *IEEE Trans. Power Electron.*, vol. 27, no. 2, pp. 782-789, Feb. 2012.

[2] M. Huang, W. Wu, Y. Yang, and F. Blaabjerg, "Step by Step Design of a High Order Power Filter for Three-Phase Three-Wire Grid-

connected Inverter in Renewable Energy System" in *Proc. PEDG 2013*, pp.1-8.

[3] A.M. Cantarellas, E. Rakhshani, D. Remon, P. Rodriguez, "Design of the LCL+Trap Filter for the Two-Level VSC Installed in a Large-Scale Wave Power Plant," in *Proc. ECCE 2013*, pp. 707-712.

[4] K. Dai, K. Duan, X. Wang, "Yong Kang Application of an LLCL Filter on Three-Phase Three-Wire Shunt Active Power Filter," in *Proc. IEEE INTELEC2012*, Sep. 2012, pp. 1-5.

[5] M. Liserre, F. Blaabjerg, and S. Hansen, "Design and control of an LCL filter-based three-phase active rectifier," *IEEE Trans. Ind. Appl.*, vol. 41, no. 5, pp. 1281–1291, Sep./Oct. 2005.

[6] F. Liu, Yan Zhou, S. Duan, J. Yin, B. Liu, F. Liu, "Parameter Design of a Two-Current-Loop Controller Used in a Grid-Connected Inverter System With LCL Filter," *IEEE Trans. Ind. Electron.*, vol. 56, no. 11, pp. 4483-4491, 2009.

[7] R. Peña-Alzola, M. Liserre, F. Blaabjerg, R. Sebastián, J. Dannehl, F.W. Fuchs, "Analysis of the Passive Damping Losses in LCL-Filter-Based Grid Converters," *IEEE Trans. Power Electron.*, vol.28, no.6, pp. 2642-2646, June 2013.

[8] W. Wu, Y. He, and F. Blaabjerg, "A New Design Method for the Passive Damped LCL- and LLCL-Filter Based Single-Phase Grid-tied Inverter," *IEEE Trans. Ind. Electron.*, vol. 60, no. 10, pp. 4339-4350, Oct. 2013.

[9] Y. Tang, P. C. Loh, P. Wang, F. H. Choo and F. Gao, "Exploring inherent damping characteristic of LCL-filters for three- phase grid-connected voltage source inverters," *IEEE Trans. Power Electron.*, vol. 27, no. 3, pp. 1433–1443, Mar. 2012.

[10] J. Dannehl, M. Liserre and F. W. Fuchs, "Filter-based active damping of voltage source converters with LCL filters," *IEEE Trans. Ind. Electron.* , vol. 58, no. 8, pp. 3623–3633, Aug. 2011.

[11] N. He, D. Xu, Y. Zhu, J. Zhang, G. Shen, Y. Zhang, J. Ma; C. Liu, "Weighted Average Current Control in a Three-Phase Grid Inverter With an LCL Filter," *IEEE Trans. Power Electron.*, vol.28, no.6, pp. 2785-2797, June 2013.

[12] J. Dannehl, F Fuchs, S Hansen, "Investigation of active damping approaches for PI-based current control of grid-connected pulse width modulation converters with LCL filters," *IEEE Trans. Ind. App.*, vol.46, no. 4, pp.1509-1517, 2010.

[13] C. Bao, X. Ruan, X. Wang, W. Li, D. Pan, and K, Weng, "Step-by-Step Controller Design for LCL-Type Grid-Connected Inverter with Capacitor–Current-Feedback Active-Damping," *IEEE Trans. Power Electron.*, vol. 29, no. 3, pp. 1239–1253, 2014.

[14] D. Pan, X. Ruan, C. bao, W. Li, X. Wang, "Capacitor-Current-Feedback Active Damping With Reduced Computation Delay for

Improving Robustness of LCL-Type Grid-Connected Inverter," *IEEE Trans. Power Electron.*, vol.29, no. 7, pp.1, 2014.

[15] S. Parker, B. McGrath , D.G. Holmes. "Regions of Active Damping Control for LCL Filters," in *Proc. IEEE ECCE 2012*, Raleigh, NC, pp. 53-60.

[16] C. Zou, B. Liu, S. Duan, and R. Li, "Influence of Delay on System Stability and Delay Optimization of Grid-Connected Inverters with LCL Filter," *IEEE Trans. Ind. Info.*, in press.

[17] C. Bao, X. Ruan, X. Wang, W. Li, D. Pan, and K, Weng, "Design of injected grid current regulator and capacitor-current-feedback active-damping for LCL-type grid-connected inverter," in *proc. ECCE 2012* , Raleigh, NC, on page(s): 579 –586.

[18] R. Pena-Alzola, M. Liserre, F. Blaabjerg, M. Ordonez, T. Kerekes, "Self-commissioning Notch Filter for Active Damping in Three Phase LCL-filter Based Grid-tie Converter," *IEEE Trans. Power Electron.*, vol. pp, in press, 2014.

[19] M. Liserre, R. Teodorescu, and F. Blaabjerg, "Stability of Photovoltaic and Wind Turbine Grid-Connected Inverters for a Large Set of Grid Impedance Values," *IEEE Trans. Power Electron.*, vol. 21, no. 1, pp. 263–272, Jan. 2006.

[20] M. Huang, P. C. Loh, W. Wu and F. Blaabjerg, "Stability Analysis and Active Damping for LLCLfilter Based Grid-Connected Inverters," in *Proc. IPEC 2014*, pp. 2610-2617.

[21] D. N. Zmood and D. G. Holmes, "Stationary frame current regulation of PWM inverters with zero steady-state error", *IEEE Trans. Power Electron.*, vol. 18, no. 3, pp. 814–822, May 2003.

[22] S. G. Parker, B. P. McGrath, D. G. Holmes, "Managing Harmonic Current Distortion for Grid Connected Converters with Low Per-Unit Filter Impedances," in *Proc. ECCE Asia*, 2013, pp. 1150-1156.

[23] M. Xue, Y. Zhang, Y. Kang, Y. Yi, S. Li, and F. Liu, "Full feed forward of grid voltage for discrete state feedback controlled grid-connected inverter with LCL filter," *IEEE Trans. Power Electron.*, vol. 27, no. 10, pp. 4234–4247, Oct. 2012.

[24] C. Zou, B. Liu, S. Duan, and R. Li, "A Feedfoward Scheme to Improve System Stability in Grid-connected Inverter with LCL Filter," in *Proc. ECCE*, 2013, pp. 4476-4480.

[25] M. A. Abusara and S. M. Sharkh, "Design of a Robust Digital Current Controller for a Grid Connected Interleaved Inverter," in *proc. IEEE ISIE*, 2010, pp. 2903-2908.

[26] A.G. Yepes, F.D. Freijedo, J. Doval-Gandoy, O. López, J. Malvar, P. Fernandez-Comesaña, "Effects of Discretization Methods on the Performance of Resonant Controllers," *IEEE Trans. Power Electron.*, vol. 25, no. 7, pp. 1692–1712, Oct. 2010.